Fachtagung "Experimentelle Strömungsmechanik"
7.–9. September 2021, Bremen

Konzentrationsmessung und Raum-Zeit-Korrelationen von passiven Skalarfeldern hoher Schmidt-Zahl in einem T-förmigen Mischer

Concentration Measurement and Space-time Correlations of High-Schmidt-number Passive Scalar Fields in a T-shaped Mixer

Huixin Li[1], Duo Xu[1,2], Tobias Schikarski[3] and Marc Avila[1,4]
1. Center of Applied Space Technology and Microgravity (ZARM), University of Bremen, Bremen, 28359, Germany
2. The State Key Laboratory of Nonlinear Mechanics, Institute of Mechanics, Chinese Academy of Sciences, Beijing, 100190, China
3. Institute of Particle Technology, Department of Chemical and Biological Engineering, Friedrich-Alexander-Universität Erlangen-Nürnberg, 91058 Erlangen, Germany
4. MAPEX Center for Materials and Processes, University of Bremen, Bremen, 28359, Germany

Email: huixin.li@zarm.uni-bremen.de

Keywords: T-mixer, PLIF, Space-time correlations, Elliptic model

Abstract
Fluid mixing is ubiquitous and indispensable in processes engineering, e.g., chemical synthesis and micro-particle synthesis. This study focuses on the mixing process of two water streams in a T-shaped mixer with a hydraulic diameter of 40 millimeters. We use planar laser-induced fluorescence to measure the concentration field approximately down to the Bachelor length scale (the smallest scale at which the passive scalar fluctuates). This method enables a detailed examination of the flow characteristics in the viscous-convective range (between the smallest velocity length scale and Batchelor scales). Our preliminary experiments were carried out with turbulent flows at the two inlets of the T-mixer. The Elliptic Approximation model was applied to the PLIF data for examination of the spatio-temporal features of the mixing in the T-mixer. We found that the space-time correlation curves for both Reynolds numbers exhibit elliptic shapes, as predicted by the Elliptic Approximation model.

Introduction

Fluid mixing is not only common in engineering applications (e.g. in chemical and aerospace engineering), but is also ubiquitous in nature (e.g. atmospheric boundary layer and ocean flows). In chemical (process) engineering, micromixing devices are used to study the mixing process and their impact on (chemical) reactions. Among a variety of mixers, the T-shaped mixing geometry has been widely used because it is easy to manufacture and exhibits good mixing efficiency. Thus, the T-shaped mixer has attracted extensive investigations of the physics of the mixing process and characterizations of the mixing performance (Camarri et al. 2020).

There are two important parameters in the T-mixer, i.e., Reynolds number and Schmidt number. With the increase of the Reynolds numbers in the T-shaped mixer, different flow regimes have been broadly identified in previous numerical and experimental studies: the steady symmetric flow, the engulfment flow and the unsteady symmetric flow, and the chaotic flow

(Camarri et al. 2020; Zhang et al. 2019; Thomas and Ameel. 2010; Fani et al. 2013 & 2014). When the Reynolds number is low, the steady and symmetric flow is dominant. Two parallel streams of fluid form and flow from the inlet channels to the outlet (Schikarski et al. 2017, Thomas and Ameel. 2010). As the Reynolds number increases, the symmetric flow state becomes unstable and is superseded by the so called *engulfment flow state*, which has been observed with planar laser-induced fluorescence (PLIF) (Hoffmann et al. 2006; Thomas and Ameel. 2010) and flow simulation (Fani et al. 2013, Schikarski et al. 2019). Within this flow regime, the symmetric flow structure is broken due to the high flow momentum of two inlets, and the shear layer in the T junction starts to engulf both flow streams. Besides, a transition Reynolds number from steady flow to unsteady engulfment flow was also reported in the literature, e.g., $Re \approx 142$ (Thomas and Ameel. 2010; Thomas et al. 2010; Engler et al. 2004), or $Re = 180 - 195$ (Zhang et al. 2017). The difference of this critical Reynolds number might arise from different setups, which is not the main point in this study. By further increasing Reynolds numbers, the flow regains symmetry but exhibits unsteady flow behaviour. Beyond ($Re > 650$), the flow in the outlet becomes eventually turbulent (Schikarski et al. 2019). A few experimental and numerical studies focused on the transition to turbulence in a T-mixer (Minakov et al. 2013; Schikarski et al. 2019). However, few studies have focused on the mixing dynamics at high Reynolds numbers ($Re > 650$) for a T-mixer (Schikarski et al. 2019).

The chaotic mixing process can be characterized by investigating the dynamic coupling between the spatial and temporal scales of motion. For this purpose, space-time correlations of the concentration are used:

$$R_c(r,\tau) = \frac{\langle \delta c(\boldsymbol{x}+r, t+\tau)\delta c(x,t)\rangle}{\sigma_c(\boldsymbol{x})\sigma_c(\boldsymbol{x}+r)}, \tag{1}$$

where $\langle ... \rangle$ denotes a space and time average, δc is the local concentration deviation from the mean, $\sigma_c(\boldsymbol{x})$ is the root-mean-square (r.m.s.) concentration at $\boldsymbol{x}$, τ is a time separation and r is a spatial separation. Here r is chosen to follow the downstream direction. Recently, based on a second-order Taylor-series expansion of space-time correlation functions, He and Zhang (2006) proposed that the obtained $R_c(r,\tau)$ has the scaling form

$$R_c(r,\tau) = R_c(r_E, 0), \tag{2}$$

with r_E being of the elliptical form,

$$r_E^2 = (r - U\tau)^2 + (V\tau)^2, \tag{3}$$

where U is a time-averaged mean-flow velocity and V is associated with a random sweeping velocity proportional to the local root-mean-square velocity (Zhao and He 2009; He et al. 2010; Zhou et al. 2011; Hogg and Ahlers 2013). The elliptical form incorporates both the Taylor hypothesis when V is small and Kraichnan's random sweeping hypothesis (Kraichnan 1964) if U vanishes. The equation (3) is named the Elliptic Approximation (EA) Model and has been verified in turbulent shear flow (He and Zhang. 2006), turbulent channel flow (Zhao and He 2009), and turbulent Rayleigh-Benard (RB) convection (Zhou et al. 2011). Recently, He et al. 2010 & 2014 extended this model to a passive temperature field in turbulent RBC, which demonstrated broad applications of the EA model into different turbulent flows. Besides, Hogg and Ahlers (2013) showed that the space-time correlation function of the shadowgraph images (the intensity of the passive scalar) also has the elliptic form, and they used the Elliptic Approximation to study the scaling behaviour of the large-scale circulation in turbulent RBC. Following the studies of He et al. 2010 & 2014 and Hogg and Ahlers 2013, $R_c(r,\tau)$ is expected to be described by the EA model in the flow in our T-mixer, which might be useful to understand the mixing flow regimes at different Reynolds numbers.

To measure the concentration, the planar laser-induced fluorescence (PLIF) technique is used in this study. In high Schmidt number turbulent flows, the small-scale interactions, particularly in the scalar fields, are difficult (or infeasible) to capture through accurate simulations (Schumacher et al. 2005). In recent years, the progress of the PLIF technique makes it possible

to visualize the smallest length scale at which the scalar fluctuates (Batchelor scale) during the mixing processes. The pixel-wise resolution of PLIF can reach down to the Batchelor scales through appropriately selecting the focal length of a camera lens and sensor resolutions of a camera. However, the thickness of the laser sheet may easily exceed the Batchelor scale along the depth direction. Miller and Dimtakis 1991 reported a LIF measurement in an axisymmetric jet flow for a range of Reynolds numbers from 2,940 to 23,400, in which they can roughly resolve 8-40 times Batchelor scales in the depth direction. Dasi et al. 2006 and Mohaghar et al. 2020 used the PLIF technique in the turbulent boundary layer and achieved the high-resolution measurements along with the depth (approximate 5 times Batchelor scales in their study). In our study, to improve the measurements in the depth direction, two efforts have been made. On the one hand, the T-mixer is enlarged to a height of 40 millimeters, where for the Reynolds number equal to 650 with the laminar-laminar inlet condition, the Bachelor scale is approximately 25 micrometers (Schikarski et al. 2017 & 2019); on the other hand, a narrow band around the focal line of the laser sheet, where the thickness of the laser sheet is about 20 micrometers, is used for the PLIF measurements to approximately reach the Batchelor scale.

This paper is organized as follows. We first give detailed descriptions of the experimental setup and the measuring technique. Further, experimental results are presented and discussed with a focus on two parts. In the first part, we estimate whether present PLIF measurements can resolve the viscous-convective range (between the Kolmogorov and Batchelor scales). In the second part, the EA Model is tested for the obtained concentration space-time correlations. The article is closed with a discussion and summary,

Experimental setup and technique

Figure 1 shows a schematic and picture of the T-shaped mixer setup, which has a dimension of $480 \times 500 \times 40\ \mathrm{mm}^3$. A test section of the T-junction was fabricated using acrylic glass, including two $200\ \mathrm{mm}$ long inlets of squared cross-sections with an inner height of $40\ \mathrm{mm}$, and a $400\ \mathrm{mm}$ long outlet with the cross-section dimension of $80\ \mathrm{mm} \times 40\ \mathrm{mm}$ (width by height). Note that the inner corners in the junction region are associated with small radii of curvature, measured smaller than $1\ \mathrm{mm}$, which has negligible effects on flow behaviour (Thomas and Ameel. 2010). Each inlet was sealed and connected to a tank through a rubber tube and an adapter. The inner diameter of the plastic tube is $20\ \mathrm{mm}$. There are two equal-sized tanks, and one is filled with water, while the other tank is filled with a mixture of water and fluorescent dye (Rhodamine 6G) to the same height level. To estimate the mean flow velocities, the volumes of water are pre-marked in the tanks. A ball valve at the outlet of each tank was used to restrict flow rates and adjust the Reynolds numbers. Similarly, the outlet channel is also connected to the same dimension rubber tube for draining. During the assembly and experiments, the entire setup was carefully levelled and the symmetry on both sides of the T junction was also ensured.

PLIF can quantitatively measure the scalar fields in two dimensions with high spatial resolution. PLIF technique was carried out to interrogate the flow at a given location ($y/\mathrm{H} = 6.25$) in the middle height of the outlet channel. A pulsed Nd:YAG-laser of 532-nm wavelength with a group of optics was used to form a horizontal laser sheet for the flow. The pixel-wise resolution along x and y direction can reach down to the Batchelor scales through the camera lens ($f = 50\ \mathrm{mm}$) and an 8-bit CCD camera with 2560×1600 pixels. The camera was placed about 1 meter above the laser sheet. However, the common thickness ($\sim 0.5\ \mathrm{mm}$) of the laser sheet is insufficient to resolve the Batchelor scales along the depth direction.

GALA e.V., Karlsruhe, Germany, ISBN 978-3-9816764-7-1

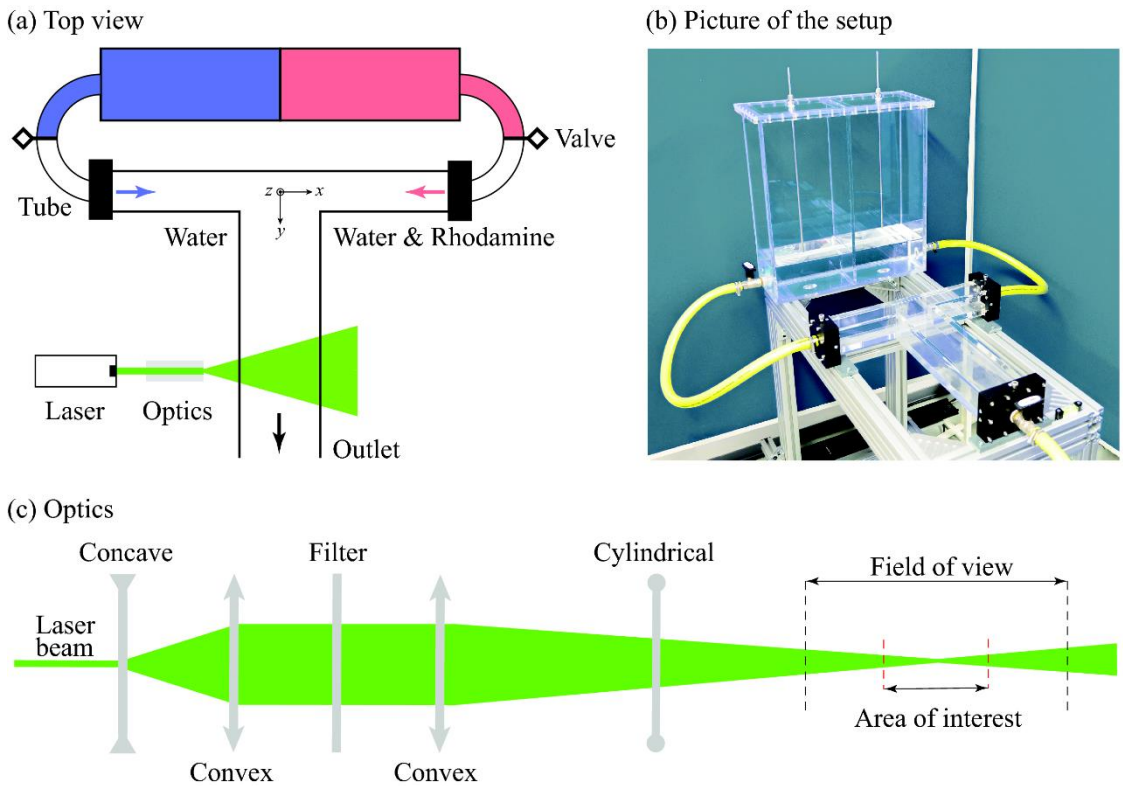

Figure 1. A sketch of a T-mixer test unit, composed of two equal-sized tanks and a T-junction section, where a PLIF measurement is taken: The left tank is for water and the right tank saves water and Rhodamine 6G. The arrows indicate the flow direction. The green parts show the laser sheet. (a) top view and (b) picture of the setup. (c) The configuration of optics to reach thin laser thickness, viewing along with the laser sheet.

In this study, to achieve a smaller thickness of the laser sheet at the measurement location, the diameter of the laser beam ($8\ \mathrm{mm}$) from the pulsed laser is expanded to $16\ \mathrm{mm}$ through a combination of two spherical lenses before being focused by a $300\ \mathrm{mm}$ focal length plano-convex lens. A filter was employed to produce a sharper Gaussian profile and further decrease the thickness of the laser sheet. These components served to focus the laser beam down to a waist diameter of approximately $0.02\ \mathrm{mm}$, and the area-of-interest (Rayleigh length) corresponding to this configuration was about $4\ \mathrm{mm}$ (Ready 1997). During the PLIF measurements, one inlet tank was doped with a passive, fluorescent dye (Rhodamine 6G) whose peak absorption and emission wavelengths are around 530 and 565 nm (Sakai et al. 2007), respectively. The respective Schmidt number is approximately 600 (Odier et al. 2014). The other tank remained undoped. Based on the hydraulic diameter of the square inlet channels and the mean velocity therein, the Reynolds numbers are $Re \approx 440$ and $Re \approx 900$ for the experiments in this study.

Results and discussion

PLIF measurements

A sample of PLIF measurements is shown in Figure 2(a), and three profiles of the dye concentration ϕ are shown in (b). The area-of-interest and the area-of-reference are marked with the same distance from the channel middle. With a sufficient number of samples, the flow statistics are assumed to be the same in two areas. The spatial gradients of the dye concentration ϕ are computed with a second-order central finite-difference scheme. The probability density function of ϕ is shown in figure 2(c), where sharper interfaces, indicated by larger ϕ,

GALA e.V., Karlsruhe, Germany, ISBN 978-3-9816764-7-1

can be resolved in the area-of-interest. Based on our present optical elements, the laser sheet in the area-of-interest is thin and could resolve smaller scales in the depth direction, however, in the area-of-reference, the laser sheet becomes thicker and the measured fluids interfaces are smeared. These preliminary PLIF measurements provide evidence that the viscous-convective range can be experimentally resolved. Further accurate, reproducible and better-controlled measurements and verification are being carried out.

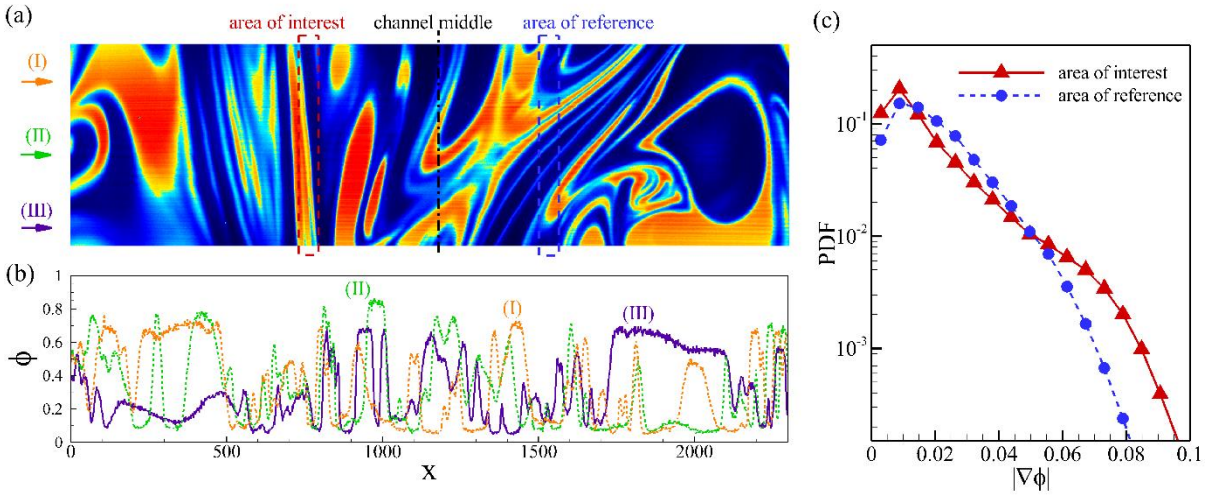

Figure 2. (a) Contours of a PLIF sample ($Re \approx 440$), where red and blue correspond to high and low concentration ϕ of fluorescent dye, respectively. (b) Three profiles of the PLIF data ϕ obtained by a horizontal cut through the cross-section (see three arrows marked in (a)). (c) Probability density function (PDF) of ϕ, where the red and blue lines correspond to the statistics from the area-of-interest and the area-of-reference (marked in a), which have the same area (40×800 pixels) and are equally distanced from the channel middle line.

Space-time correlations of the concentration field

We studied the properties of space-time correlations for the concentration along the downstream direction in the area-of-interest. Figure 3 shows the contours of the measured $R_c(r,\tau)$ for $Re \approx 440$ and $Re \approx 900$. The correlations function $R_c(r,\tau)$ has by definition a maximum in the origin ($R_c(0,0) = 1$), and decays monotonically to zero at large values of r and τ. For the present ranges of r and τ, contour lines with the same isolevels close to the center appear to be elongated and closed curves. Indeed, they depict an elliptical curve shape, which thus can be described by equation (3). For $Re \approx 900$, the isocorrelation contours of the measured $R_c(r,\tau)$ are elongated strongly along the of r and τ, compared to the contours at $Re \approx 440$.

To determine the characteristic velocities U and V in equation (2) and (3), from the conditions $\partial r_E/\partial r = 0$ and $\partial r_E/\partial \tau = 0$, we respectively have,

$$r_p = U\tau \quad \text{and} \quad \tau_p = [U/(U^2 + V^2)]r, \tag{4}$$

Here, r_p maximizes $R_c(r,\tau)$ for a given τ. And τ_p is the peak position at which $R_c(r,\tau)$ reaches its maximum value for a fixed separation r (He et al. 2010; Zhou et al. 2011; Hogg and Ahlers. 2013). As shown in Figure 4, r_p changes linearly with τ and τ_p has a linear trend with r, as predicted by equation (4). The fitting U and V for $Re \approx 440$ are $24.51\ \mathrm{mm/s}$ and $3.53\ \mathrm{mm/s}$, respectively. While for $Re \approx 900$, we found the fitting $U = 43.91\ \mathrm{mm/s}$ and $V = 4.36\ \mathrm{mm/s}$. The large ratio of U and V at $Re \approx 900$ leads to that the contour curves are elongated and approach the straight lines, as shown in figure 3(b). Besides, these two U are approximately equal to the measured mean velocities in the outlet channel ($22.26\ \mathrm{mm/s}$ and $45.75\ \mathrm{mm/s}$, respectively), which roughly indicates that the EA model holds for the present flow.

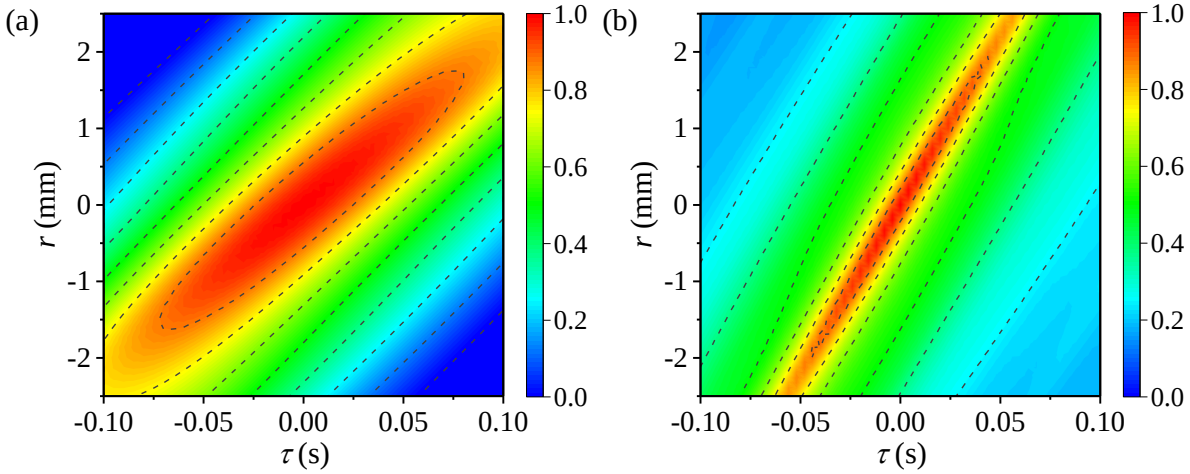

Figure 3. Space-time correlations $R_c(r,\tau)$ as a function of r and τ measured in the area-of-interest for $Re \approx 440$ (a) and $Re \approx 900$ (b).

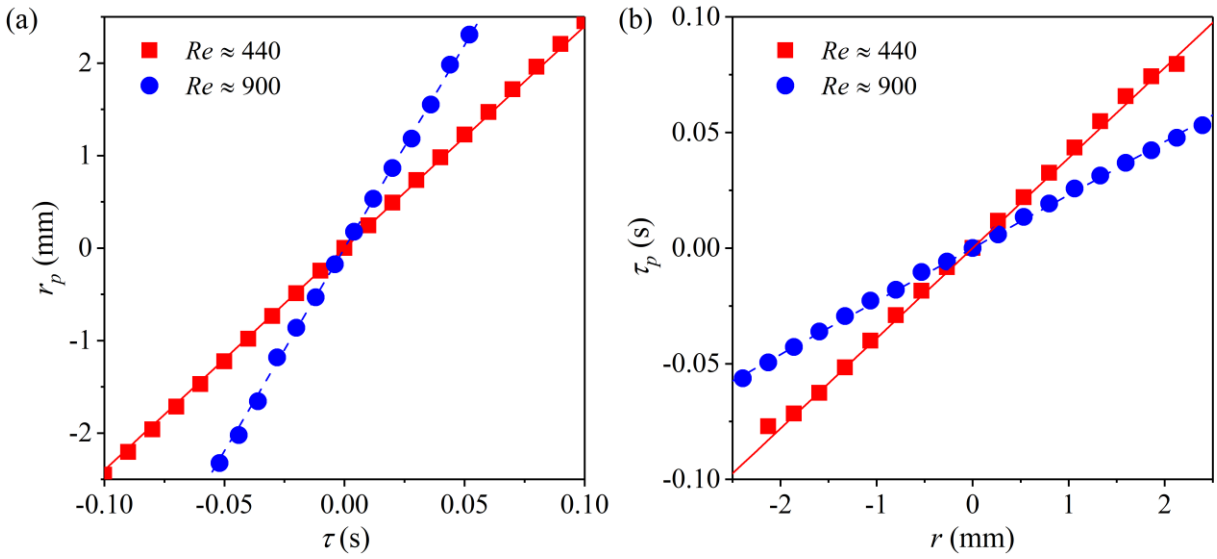

Figure 4. (a) The measured peak position r_p as a function of τ for $Re \approx 440$ (square) and $Re \approx 900$ (circle). The solid and dashed lines show the fitted linear function, $r_p = U\tau$, with $U = 24.51\ \mathrm{mm/s}$ for $Re \approx 440$ and $U = 43.91\ \mathrm{mm/s}$ for $Re \approx 900$, respectively. (b) The measured peak position τ_p as a function of r. The solid line and dashed line show the fitted linear function, $\tau_p = [U/(U^2+V^2)]r$, with $U/(U^2+V^2) = 0.04\ \mathrm{s/mm}$ for $Re \approx 440$ and $U/(U^2+V^2) = 0.023\ \mathrm{s/mm}$ for $Re \approx 900$, respectively. All data were obtained in the area-of-interest.

Summary

In this study, we designed a new high-resolution PLIF measurement facility which allows us to investigate the mixing behavior of high Schmidt number turbulent flows. We aim to investigate the mixing process in micromixing devices subject to many mixing-controlled chemical processes. The probability density function of concentration gradient provides good evidence that present optics and T-shaped setup can reach high resolution along with the depth of the laser sheet. Subsequently, for the obtained concentration field, the space-time correlations were calculated and we also test the Elliptic Approximation model of He and Zhang. 2006 for the correlations. At $Re \approx 440$, the correlation curves approximately have elliptic shapes, as predicted by the EA model, while at $Re \approx 900$, the increase of the flow mean velocity is larger

than that of the velocity fluctuation in the outlet channel seen by a strong elongation of the correlation curves. Remarkably, both mean flow velocities obtained from the EA model are close to the values from the measurements. In the near future, we will extend our study by improving the inflow profiles and extending the statistical evaluations at different Re.

Acknowledgements

This work was supported by the Deutsche Forschungsgemeinschaft (DFG, German Science Foundation) - INST 144/464. H. Li gratefully acknowledges the support from the Chinese Scholarship Council (No. CSC201804930530).

Reference

Thomas, S., Ameel, T.A., 2010: "An Experimental Investigation of Moderate Reynolds Number Flow in a T-Channel", Experiments in Fluids, 49(6), pp.1231-1245

Thomas, S., Ameel, T.A., Guilkey, J., 2010: "Mixing Kinematics of Moderate Reynolds Number Flows in a T-channel", Physics of Fluids, 22(1), pp. 013601

Hoffmann, M., Schlüter, M., Räbiger, N., 2006: "Experimental Investigation of Liquid-liquid Mixing in T-shaped Micro-mixers Using μ-LIF and μ-PIV", Chemical Engineering Science, 61(9), pp. 2968-2976

Fani, A., Camarri, S., Salvetti, M.V. 2013: "Investigation of the Steady Engulfment Regime in a Three-dimensional T-mixer", Physics of Fluids, 25(6), pp. 064102.

Fani, A., Camarri, S., Salvetti, M.V., 2014: "Unsteady Asymmetric Engulfment Regime in a T-mixer", Physics of Fluids, 26(7), pp. 074101

Camarri, S., Mariotti, A., Galletti, C., Brunazzi, E., Mauri, R., Salvetti, M.V. 2020: "An Overview of Flow Features and Mixing in Micro T and Arrow Mixers", Industrial & Engineering Chemistry Research, 59(9), pp. 3669-3686

Engler, M., Kockmann, N., Kiefer, T., Woias, P., 2004: "Numerical and Experimental Investigations on Liquid Mixing in Static Micromixers", Chemical Engineering Journal, 101(1-3), pp. 315-322

Schikarski, T., Peukert, W., Avila, M., 2017: "Direct Numerical Simulation of Water–ethanol Flows in a T-mixer", Chemical Engineering Journal, 324, pp. 168-181

Minakov, A., Rudyak, V., Dekterev, A., Gavrilov, A., 2013: Investigation of Slip Boundary Conditions in the T-shaped Microchannel. International Journal of Heat and Fluid Flow, 43, pp. 161-169

Schikarski, T., Trzenschiok, H., Peukert, W., Avila, M., 2019: "Inflow Boundary Conditions Determine T-mixer Efficiency", Reaction Chemistry & Engineering, 4(3), pp. 559-568

Zhang, J.W., Liu, S.F., Cheng, C., Li, W.F., Xu, X.L., Liu, H.F., Wang, F.C., 2019: "Investigation of Three-dimensional Flow Regime and Mixing Characteristic in T-jet Reactor", Chemical Engineering Journal, 358, pp. 1561-1573

Schumacher, J., Sreenivasan, K.R. Yeung, P.K, 2005: "Very Fine Structures in Scalar Mixing", Journal of Fluid Mechanics, 531, pp. 113-122

He, G.W., Zhang, J.B., 2006: "Elliptic Model for Space-time Correlations in Turbulent Shear Flows", Physical Review E, 73(5), pp. 055303

Zhao, X., He, G.W., 2009: "Space-time Correlations of Fluctuating Velocities in Turbulent Shear Flows", Physical Review E, 79(4), pp. 046316

Kraichnan, R.H. 1964: "Kolmogorov's hypotheses and Eulerian turbulence theory", Physics of Fluids, 7, pp.1723-1734

Zhou, Q., Li, C.M., Lu, Z.M., Liu, Y.L., 2011: "Experimental Investigation of Longitudinal Space–time Correlations of the Velocity Field in Turbulent Rayleigh–Bénard Convection", Journal of Fluid Mechanics, 683, pp. 94-111

He, G., Jin, G., Yang, Y., 2017: "Space-time Correlations and Dynamic Coupling in Turbulent Flows", Annual Review of Fluid Mechanics, 49, pp. 51-70

He, X., Shang, X.D., Tong, P., 2014: "Test of the Anomalous Scaling of Passive Temperature Fluctuations in Turbulent Rayleigh-Bénard Convection with Spatial Inhomogeneity", Journal of Fluid Mechanics, 753, pp. 104-130

He, X., Tong, P., 2014: "Space-time Correlations in Turbulent Rayleigh-Bénard Convection", Acta Mechanica Sinica, 30(4), pp. 457-467

He, X., He, G., Tong, P., 2010: "Small-scale Turbulent Fluctuations beyond Taylor's Frozen-flow Hypothesis", Physical Review E, 81(6), pp. 065303
Hogg, J., Ahlers, G., 2013: "Reynolds-number Measurements for Low-Prandtl-number Turbulent Convection of Large-aspect-ratio Samples", Journal of Fluid Mechanics, 725, pp. 664-680
Dasi, L.P., Schuerg, F., Webster, D.R., 2007: "The Geometric Properties of High-Schmidt-number Passive Scalar Iso-surfaces in Turbulent Boundary Layers", Journal of Fluid Mechanics, 588, pp. 253-277
Mohaghar, M., Dasi, L.P., Webster, D. R., 2020: "Scalar Power Spectra and Turbulent Scalar Length Scales of High-Schmidt-number Passive Scalar Fields in Turbulent Boundary Layers", Physical Review Fluids, 5(8), pp. 084606
Miller, P.L., Dimotakis, P.E., 1991: "Stochastic Geometric Properties of Scalar Interfaces in Turbulent Jets", Physics of Fluids, 3(1), 168-177
Ready, J. F., 1997: "Industrial Applications of Lasers", Elsevier.
Sakai, M., Ohmori, T., Fujii, M. 2007: "Two-color Picosecond Time-resolved Infrared Super-resolution Microscopy", Handai Nanophotonics, 3, pp. 189-195
Odier, P., Chen, J., Ecke, R., 2014: "Entrainment and Mixing in a Laboratory Model of Oceanic Overflow", Journal of Fluid Mechanics, 746, pp. 498-535

GALA e.V., Karlsruhe, Germany, ISBN 978-3-9816764-7-1